Interpretation of suprathermal emission at deuteron cyclotron harmonics from deuterium NBI plasmas in KSTAR

R O Dendy[1,2], B Chapman[2], G S Yun[3], S C Chapman[2], K G McClements[1], S G Thatipamula[3], M H Kim[3] and A Zalzali[2]

[1]*CCFE, Culham Science Centre, Abingdon, Oxfordshire OX14 3DB, UK*

[2]*Centre for Fusion, Space and Astrophysics, Department of Physics, Warwick University, Coventry CV4 7AL, UK*

[3]*Department of Physics, Pohang University of Science and Technology, Pohang 37673, Korea*

1. Introduction

Intense suprathermal radiation, with spectral peaks at multiple harmonics of the deuteron cyclotron frequency, is detected[1,2] from the outer midplane edge of KSTAR deuterium plasmas that are heated by tangential neutral beam injection (NBI) of 100keV deuterons. We identify[3] how this deuterium ion cyclotron emission (ICE) is generated, and distinguish this signal from the ICE driven by fusion-born protons in KSTAR deuterium plasmas[4,5]. We first combine particle orbit studies in approximate KSTAR magnetic field geometry with an analytical treatment of the magnetoacoustic cyclotron instability (MCI)[6,7], to identify the sub-population of freshly ionised NBI deuterons that can excite deuterium ICE by the MCI. These deuterons are then represented as an energetic minority, together with the majority thermal deuteron population and electrons, in kinetic particle-in-cell (PIC)[8] computational studies where all particle gyro-orbits are fully resolved. The PIC approach solves the Maxwell-Lorentz equations for many millions of interacting particles, with the self-consistently evolving electric and magnetic fields. It enables us to study the collective relaxation of the NBI deuterons through the linear phase of the MCI and deep into its saturated regime. The Fourier transform of the excited fields displays strong spectral peaks at multiple successive deuteron cyclotron harmonics, mapping well to the observed KSTAR deuterium ICE spectra. The time-evolution of the energy densities of the particle populations and field components in the PIC computations further supports our identification of the driving sub-population of NBI deuterons, whose relaxation through the MCI generates the observed deuterium ICE signal. We conclude that the physical origin of this signal in KSTAR is broadly the same as the NBI-driven ICE seen in TFTR tokamak[9] and LHD stellarator plasmas[10,11]. Its spatially localised character suggests that planned ion beam-plasma experiments in simpler magnetic geometries could also generate ICE of this kind. The success of this approach will assist future interpretation of other contemporary ICE measurements[12,13], which may be generated simultaneously by fusion-born and NBI ions, and from the plasma core as well as the edge.

2. Identification of the ICE-generating sub-population of NBI deuterons

Generation of ICE by the MCI requires the localised existence of a strongly non-Maxwellian velocity distribution for the energetic minority ions in the emitting region. The latter is identified by matching spectral peak frequencies to local magnetic field strength, on the basis that the peaks correspond to successive deuteron cyclotron harmonics. Figure 1 displays the results of orbit studies[3] showing that the drift orbits of NBI deuterons whose gyro-orbits are nearly, but not exactly, perpendicular to the magnetic field can create the necessary population inversion at the outer midplane edge. Analytical studies[3] confirm that this distribution is likely to be unstable against the MCI under KSTAR edge plasma conditions.

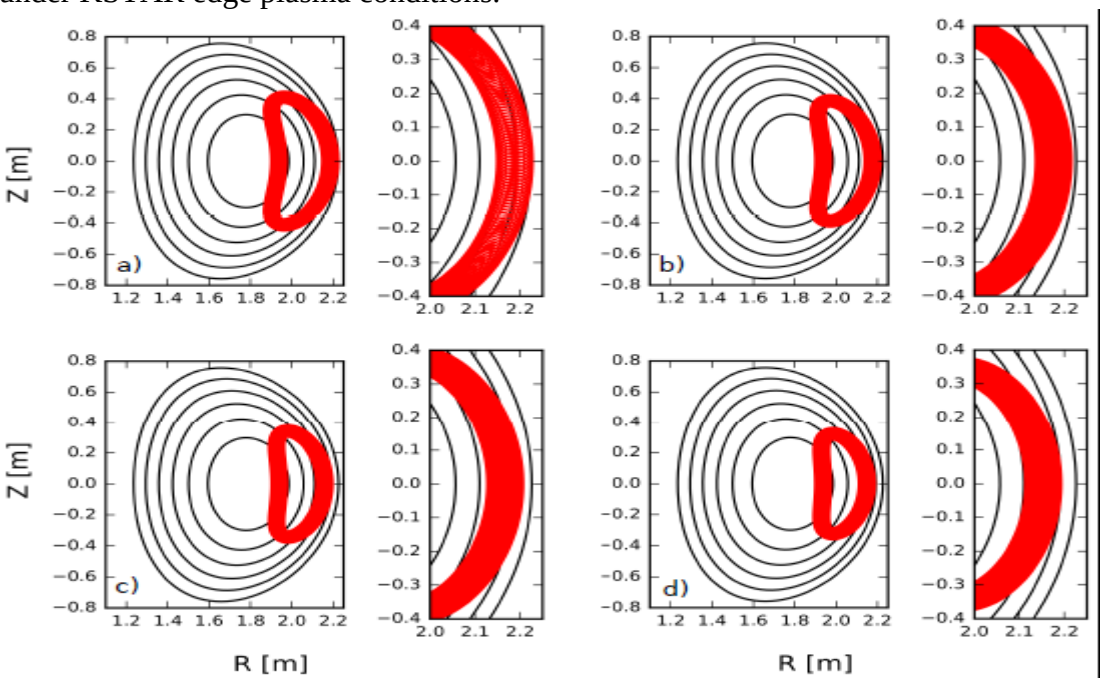

Fig.1 Poloidal projection of 100keV NBI deuteron orbits calculated using a test particle code with a Solov'ev approximation to a typical KSTAR equilibrium. Particle orbits are initialised near the core for four pitch angles in the range $80^o < \varphi < 84^o$. Full orbits together with insets of the edge region are shown. Panels a) to d) are for initial pitch angles of 80^o, 81^o, 83^o, and 84^o respectively. Reproduced from Ref.[3].

3. Results of particle-in-cell computations

We initialise the PIC computations with an energetic deuteron minority, whose distribution and parameters are derived from Sec.2, embedded in the thermal plasma. The system then spontaneously relaxes at the level of Maxwell-Lorentz particle kinetics, giving time traces for the different components of particle and self-consistent field energy that are shown in Fig.2. These exhibit characteristic MCI phenomenology. Figure 2 shows that the primary energy flow is from the NBI deuterons to the thermal deuterons, whose kinetic oscillation helps support the field oscillations excited by the MCI. These field oscillations include, with comparable magnitude, an electromagnetic component $(\Delta B_z)^2$ and an electrostatic component $(E_x)^2$. The electrostatic component involves electron kinetics which are fully captured in our PIC model.

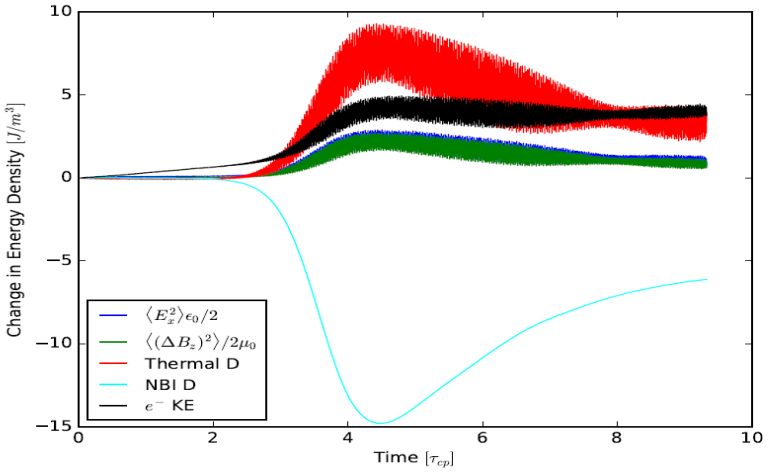

Fig.2 Time evolution of the change in energy density of particles and electric and magnetic fields, from a PIC simulation with $n_{NBI}/n_{thermal} = \xi = 10^{-3}$. Top (red) Change in kinetic energy density of the thermal bulk plasma deuterons; (black) change in energy density of the electrons; (blue) energy density of the electrostatic field E_x; (green) energy density of the magnetic field perturbation ΔB_z; (cyan) change in kinetic energy density of the minority energetic NBI deuterons. Time is normalised to the deuteron gyro period τ_{cD}. Reproduced from Ref.[3].

The spatiotemporal Fourier transform of the excited $(\Delta B_z)^2$ is shown in Fig.3. The sweep of the fast Alfvén wave from bottom left to top right is intersected by cyclotron harmonic waves at successive deuteron harmonics. The phase velocity of the fast Alfvén wave ~ v_A, and this exceeds the speed v_{NBI} of the NBI deuterons which is plotted as a blue diagonal line. Wave excitation is strongest in the wedge between v_A and v_{NBI}, and in particular where cyclotron harmonic waves intersect the fast Alfvén wave.

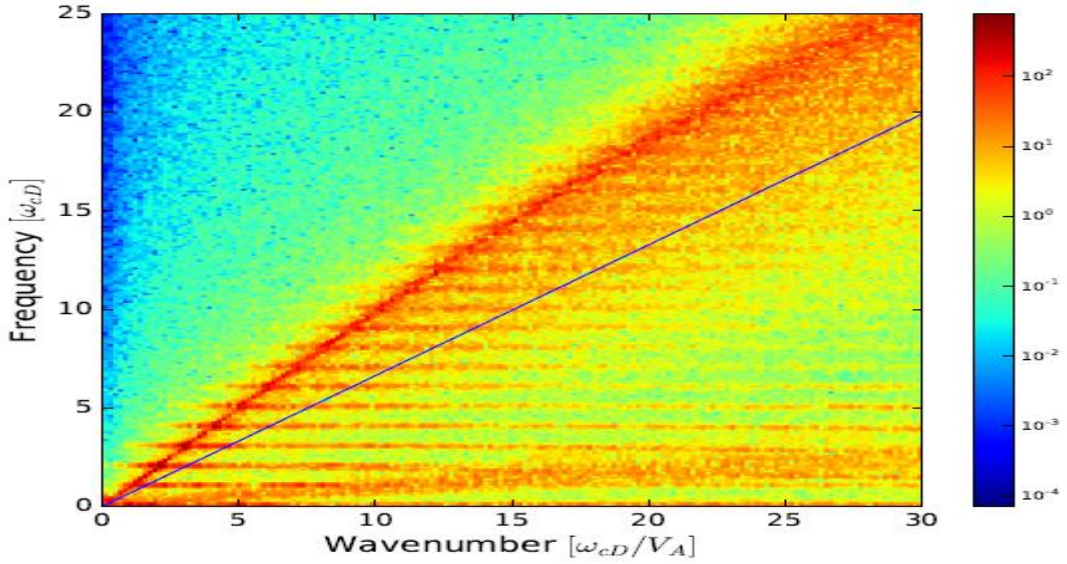

Fig.3 Distribution of energy in the oscillatory part ΔB_z of the B_z field component across frequency-wavenumber space from a PIC simulation with $\xi = 10^{-2}$, $T_e = T_D = 1$keV, $B_{0z} = 1{:}44$T, $n_e = 2.5 \times 10^{19}$m^{-3}, and a 100keV minority NBI deuteron population. The intervals span $0 < x < 50{,}000\lambda_D$ and $0 < t < 5\tau_{cD}$. Shading indicates the $\log_{10}$ of the spectral density. Reproduced from Ref.[3].

4. Conclusions: comparison of simulated and measured ICE spectra

We obtain simulated ICE frequency spectra by integrating spatiotemporal Fourier transforms, such as Fig.3, over wavenumber. Figure 4 provides two comparisons of simulated and measured ICE spectra for KSTAR deuterium NBI plasmas. We conclude that the physics underlying our computational approach aligns well with the observed ICE phenomenology in KSTAR.

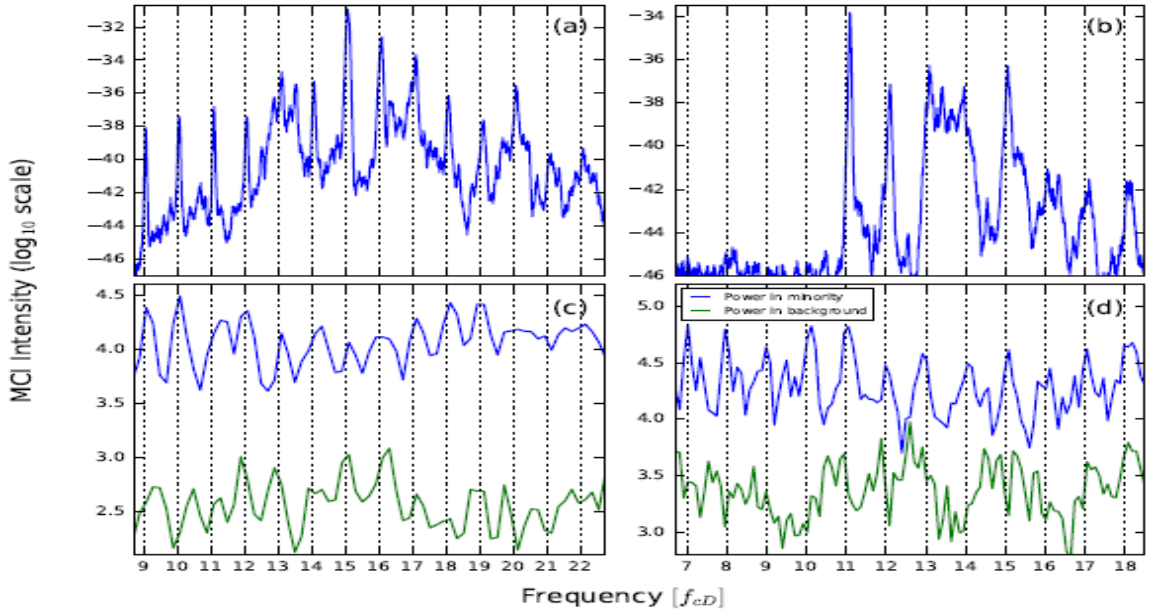

Fig.4 Top: Measured spectral intensity of ICE from KSTAR deuterium plasmas with 100keV deuteron NBI heating[2], $n_e = 2.5 \times 10^{19}m^{-3}$ and $T_e = T_D = 1keV$. (a)Plasma 16176: $B_0 = 1.84T$, local $f_{cD} = 11.1MHz$; (b) Plasma 11474: $B_0 = 2.27T$, local $f_{cD} = 14.0MHz$. Bottom: Blue traces are outputs of PIC simulations of the spectral intensity of the fluctuating B_z field energy density, resulting from relaxation of a minority 100keV deuteron ring-beam population in thermal deuterium plasma. Green traces are the noise baseline. The simulation parameters of (c) and (d) map to (a) and (b) respectively. Reproduced from Ref.[3].

[1] S G Thatipamula, G S Yun *et al*., 2016 Plasma Phys. Control. Fusion **58** 065003
[2] M Kim, S Thatipamula *et al*., 2018 Nucl. Fusion **58** 096034
[3] B Chapman, R O Dendy *et al*., 2019 Nucl. Fusion submitted
[4] B Chapman, R O Dendy *et al*., 2017 Nucl. Fusion **57** 124004
[5]B Chapman, R O Dendy *et al*., 2018 Nucl. Fusion **58** 096027
[6] R O Dendy, C N Lashmore-Davies *et al*., 1994 Phys. Plasmas **1** 1918
[7] L Carbajal, R O Dendy *et al*., 2017 Phys. Rev. Lett. **118** 105001
[8] T D Arber, K Bennett *et al*., 2015 Plasma Phys. Control. Fusion **57** 113001
[9] S Cauffman, R Majeski et al., 1995 Nucl. Fusion **35** 1597
[10] B C G Reman, R O Dendy, T Akiyama *et al*., 2016 EPS Conference Proceedings P2.041
[11] B C G Reman, R O Dendy *et al*., 2019 Nucl. Fusion accepted
[12] R Ochoukov, R Bilato, V Bobkov *et al*., 2019 Nucl. Fusion **59** 014001
[13] K E Thome, D C Pace *et al*., 2019 Nucl. Fusion accepted https://doi.org/10.1088/1741-4326/ab20e7

This work was carried out within the framework of the EUROfusion Consortium and received funding from the Euratom research and training programme 2014-2018 and 2019-2020 under grant agreement No 633053. Support was received from the RCUK Energy Programme grant no. EP/P012450/1 and NRF Korea grant no. 2014M1A7A1A03029881. The views and opinions expressed herein do not necessarily reflect those of the European Commission.